



HAL
open science

Increased surface P2X4 receptor regulates anxiety and memory in 3 P2X4 internalization-defective knock-in mice

Eléonore Bertin, Thomas Deluc, Estelle Toulmé, Kjara S Pilch, Audrey Martinez, Johan-Till Pougnet, Evelyne Doudnikoff, Anne-Emilie Allain, Philine Bergmann, Marion Russeau, et al.

► **To cite this version:**

Eléonore Bertin, Thomas Deluc, Estelle Toulmé, Kjara S Pilch, Audrey Martinez, et al.. Increased surface P2X4 receptor regulates anxiety and memory in 3 P2X4 internalization-defective knock-in mice. *Molecular Psychiatry*, 2020, <10.1038/s41380-019-0641-8>. <hal-03003954>

HAL Id: hal-03003954

<https://hal.science/hal-03003954v1>

Submitted on 13 Nov 2020

HAL is a multi-disciplinary open access archive for the deposit and dissemination of scientific research documents, whether they are published or not. The documents may come from teaching and research institutions in France or abroad, or from public or private research centers.

L'archive ouverte pluridisciplinaire **HAL**, est destinée au dépôt et à la diffusion de documents scientifiques de niveau recherche, publiés ou non, émanant des établissements d'enseignement et de recherche français ou étrangers, des laboratoires publics ou privés.



HAL Authorization



Increased surface P2X4 receptor regulates anxiety and memory in P2X4 internalization-defective knock-in mice

Eléonore Bertin^{1,2} · Thomas Deluc^{1,2,3} · Kjara S. Pilch^{1,2} · Audrey Martinez^{1,2} · Johan-Till Pougnet^{1,2} · Evelyne Doudnikoff^{1,2} · Anne-Emilie Allain^{4,5} · Philine Bergmann⁶ · Marion Russeau⁷ · Estelle Toulmé^{1,2} · Erwan Bezard^{1,2} · Friedrich Koch-Nolte⁶ · Philippe Séguéla³ · Sabine Lévi⁷ · Bruno Bontempi^{1,2} · François Georges^{1,2} · Sandrine S. Bertrand^{4,5} · Olivier Nicole^{1,2} · Eric Boué-Grabot^{1,2}

Received: 16 September 2019 / Revised: 10 December 2019 / Accepted: 12 December 2019
© The Author(s), under exclusive licence to Springer Nature Limited 2020

Abstract

ATP signaling and surface P2X4 receptors are upregulated selectively in neurons and/or glia in various CNS disorders including anxiety, chronic pain, epilepsy, ischemia, and neurodegenerative diseases. However, the cell-specific functions of P2X4 in pathological contexts remain elusive. To elucidate P2X4 functions, we created a conditional transgenic knock-in P2X4 mouse line (Floxed P2X4mCherryIN) allowing the Cre activity-dependent genetic swapping of the internalization motif of P2X4 by the fluorescent mCherry protein to prevent constitutive endocytosis of P2X4. By combining molecular, cellular, electrophysiological, and behavioral approaches, we characterized two distinct knock-in mouse lines expressing noninternalized P2X4mCherryIN either exclusively in excitatory forebrain neurons or in all cells natively expressing P2X4. The genetic substitution of wild-type P2X4 by noninternalized P2X4mCherryIN in both knock-in mouse models did not alter the sparse distribution and subcellular localization of P2X4 but increased the number of P2X4 receptors at the surface of the targeted cells mimicking the pathological increased surface P2X4 state. Increased surface P2X4 density in the hippocampus of knock-in mice altered LTP and LTD plasticity phenomena at CA1 synapses without affecting basal excitatory transmission. Moreover, these cellular events translated into anxiolytic effects and deficits in spatial memory. Our results show that increased surface density of neuronal P2X4 contributes to synaptic deficits and alterations in anxiety and memory functions consistent with the implication of P2X4 in neuropsychiatric and neurodegenerative disorders. Furthermore, these conditional P2X4mCherryIN knock-in mice will allow exploring the cell-specific roles of P2X4 in various physiological and pathological contexts.

These authors contributed equally: Eléonore Bertin, Thomas Deluc, Kjara S. Pilch

Supplementary information The online version of this article (<https://doi.org/10.1038/s41380-019-0641-8>) contains supplementary material, which is available to authorized users.

✉ Eric Boué-Grabot
eric.boue-grabot@u-bordeaux.fr

- 1 Université de Bordeaux, Institut des Maladies Neurodégénératives, UMR 5293, F-33000 Bordeaux, France
- 2 CNRS, Institut des Maladies Neurodégénératives, UMR 5293, F-33000 Bordeaux, France
- 3 Department of Neurology and Neurosurgery, Montreal Neurological Institute, Alan Edwards Centre for Research on Pain, McGill University, Montreal, QC H3A 2B4, Canada

Introduction

The release and extracellular action of ATP are a widespread mechanism for cell-to-cell communication in living organisms through activation of P2X and P2Y receptors expressed at the cell surface of most tissues, including the nervous system [1]. Several P2X receptors (P2X) are

- 4 Université de Bordeaux, Institut de Neurosciences Cognitives et Intégratives d'Aquitaine, UMR5287, F-33000 Bordeaux, France
- 5 CNRS, Institut de Neurosciences Cognitives et Intégratives d'Aquitaine, UMR5287, F-33000 Bordeaux, France
- 6 Institute of Immunology, University Medical Center Hamburg-Eppendorf, Martinistr. 52, D-20246 Hamburg, Germany
- 7 INSERM UMR-S 1270, Sorbonne Université, Institut du Fer à Moulin, 75005 Paris, France

expressed in the central nervous system (CNS) with varying distributions in neurons as well as in glia [2–4]. P2X receptors are ATP-gated cation channels and their activation by ATP, co-released by neurons with other neurotransmitters [5, 6] or released as a gliotransmitter by astrocytes [7–9], has profound modulatory actions at synapses [1, 10, 11]. Among the seven P2X subunits, P2X4 displays high calcium permeability [12, 13] and a widespread distribution in CNS neurons and glial cells as well as in peripheral tissues [14–16]. Nevertheless P2X4 expression in the brain is sparse [15] and its contribution to the synaptic modulation in normal conditions remains debated [17, 18]. A growing body of evidence suggests that upregulated P2X4 expression plays important roles in various CNS disorders including chronic pain and neurodegenerative diseases such as Alzheimer’s disease (AD) or amyotrophic lateral sclerosis (ALS) [19–26]. In the healthy organism, P2X4 is constitutively internalized by the interaction between the adapter protein 2 (AP2) and a noncanonical endocytosis motif in the C-tail of P2X4 subunit [27, 28]. As a result, P2X4 is found preferentially in intracellular compartments ensuring a low surface expression not only in neurons, but also in microglia and macrophages [29–32]. Intracellular P2X4 may promote vesicle fusion of endosomes or lysosomes [32, 33]. Importantly, intracellular P2X4 pools can be mobilized and trafficked to the cell surface [31, 34], consistent with the critical role of increased P2X4 surface expression in pathological states [19, 21, 24–26, 35–37]. The specific increase in P2X4 expression and surface trafficking in spinal microglia is critical for the pathogenesis of chronic pain [24, 38–41]. Increased P2X4 expression and surface density in neurons have been observed in the hippocampus or in the spinal cord of AD or ALS mouse models, respectively, suggesting that upregulated P2X4 may contribute to synaptic dysfunction and/or cell death in AD or ALS [23, 25, 26, 35]. However, the extent of the upregulated surface P2X4 state and the cell-specific functions of P2X4 in the pathological context remain elusive.

Here we report the development of conditional knock-in (P2X4mCherryIN) mice mimicking a pathological increase of surface P2X4. We show that the increase of P2X4 at the surface of excitatory neurons decreases anxiety, impairs memory processing, and alters activity-dependent synaptic plasticity phenomena in the hippocampus suggesting that upregulation of neuronal P2X4 observed in AD [25] may have key roles in AD pathogenesis. Overall, we provide an innovative knock-in P2X4 model to study the functional contributions of upregulated P2X4 in specific cells of the nervous system but also in peripheral tissues throughout the body.

Materials and methods

Experimental model

The *P2rx4* conditional knock-in mouse line was established at the MCI/ICS (Mouse Clinical Institute, France). *Xenopus* oocytes were isolated as described [42, 43]. Cultures of hippocampal neurons were prepared as described [44] with some modifications. Peritoneal cells were isolated as described [45] (see Supplementary information).

Immunofluorescence and microscopy

Immunofluorescence studies of neurons, macrophages, brain immunohistochemistry, and image acquisition are described in the Supplementary and electron microscopy (E. M.) was performed as previously described [46] (see Supplementary information).

Biotinylation assays and immunoblotting

Surface biotinylation experiments were performed as described previously [8, 43, 47] from injected *Xenopus* oocytes, mouse peritoneal macrophages, and hippocampal cell cultures (see Supplementary information).

Electrophysiology

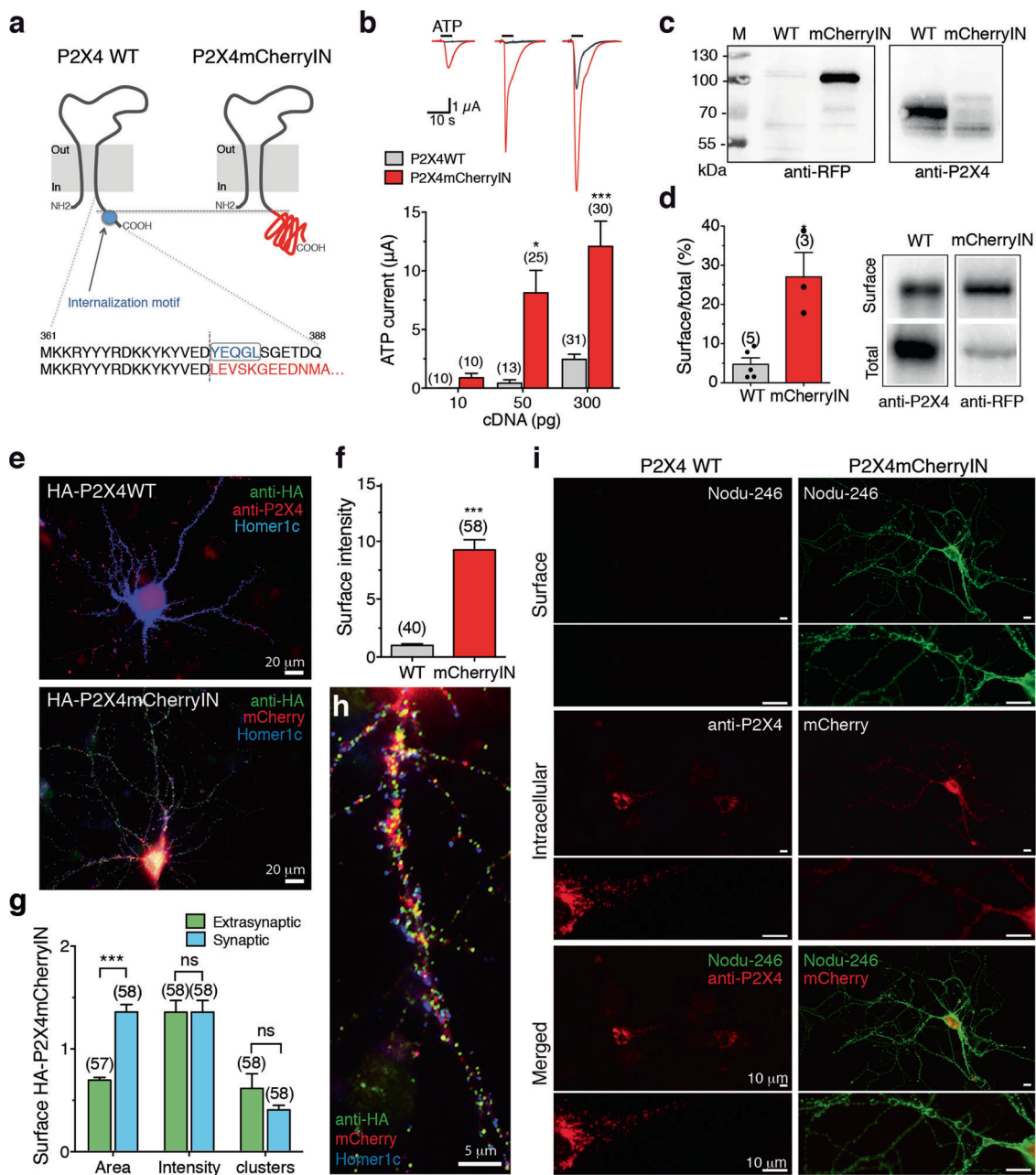
Extracellular field recordings and induction of synaptic plasticity in hippocampal brain slices are described in the Supplementary. Two-electrode voltage-clamp recordings from *Xenopus* oocyte were performed as previously described (see Supplementary information).

Mouse behavior

Open field procedure, novel object recognition test [48, 49], elevated plus maze [50], the Y-maze two-trial procedure [51], and spatial memory testing conducted in an eight-arm radial maze are described in the Supplementary information.

Quantification and statistical analysis

The number of independent experiments or animals (n), the statistical test used for comparison and the statistical significance (p values) are specified for each figure panel in the corresponding figure legend. Data are presented as mean \pm s.e.m. Data were analyzed and graphs were generated using GraphPad Prism.



Results

Substitution of the internalization motif of P2X4 by mCherry protein increases surface density of functional P2X4 receptors

Mutation or ablation of the endocytosis motif of P2X4 (Y³⁷⁸xxGL) was previously shown to increase the surface trafficking of P2X4 without altering its functional properties [28, 43]. We generated a P2X4mCherryIN construct in which the endocytosis motif of mouse wild-type (WT) P2X4 was suppressed by swapping the last 11 amino acids in the C-tail of P2X4 with the sequence coding for the red

fluorescent protein mCherry (Fig. 1a). ATP-evoked currents recorded from P2X4WT or P2X4mCherryIN expressing *Xenopus* oocytes (Fig. 1b) showed that P2X4mCherryIN response amplitudes were significantly larger than those recorded from P2X4WT (Fig. 1b). We next examined the surface level of P2X4WT and P2X4mCherryIN by biotinylation assays and western blotting from oocytes (Fig. 1c, d). Anti-P2X4 antibodies allowed the detection of P2X4WT (70 kDa) but not P2X4mCherryIN (the anti-P2X4 epitope (amino acids 370–388) is deleted in P2X4mCherryIN constructs). P2X4mCherryIN was detected using anti-RFP antibodies showing a band at 100 kDa in agreement with the fusion of mCherry (30 kDa) to P2X4 (Fig. 1c). Surface/total

◀ **Fig. 1 Substitution of the internalization motif of P2X4 by mCherry increases ATP current density and surface expression of P2X4 receptors.** **a** Schematic representation of the mouse P2X4 subunit topology and C-terminal sequence of wild-type P2X4 (WT) and P2X4mCherryIN subunits. The AP2 binding site (blue circle) within the C-terminal sequence of mouse P2X4WT was exchanged for the red fluorescent protein mCherry sequence (P2X4) preventing clathrin-dependent internalization. **b** Representative superimposed currents evoked by applications of ATP (100 μ M, 5 s) from oocytes expressing wild-type P2X4 (WT) (black traces) or P2X4mCherryIN receptors (red traces). Bar graphs of the mean amplitude of ATP current recorded from oocytes expressing P2X4WT or P2X4mCherryIN as a function of the quantity of injected cDNAs. Recordings were performed the same day (2 or 3 days) postnuclear injection. Error bars represent s.e.m., the number of cells is indicated in parentheses, $**p < 0.01$, $***p < 0.001$, one-way ANOVA and Tukey's post hoc test. Blockade of P2X4 internalization induced an approximately sevenfold increase in ATP current amplitudes. **c** Specific detection by western blots of total proteins from oocytes expressing P2X4WT (70 kDa) or P2X4mCherryIN (100 kDa) with anti-P2X4 or anti-RFP antibodies, respectively. **d** Representative immunoblots of total and surface biotinylated proteins from oocytes expressing P2X4WT (WT) or P2X4mCherryIN (mCherryIN) using anti-P2X4 or anti-RFP antibodies. Bars represent mean \pm s.e.m. of the surface/total ratio of P2X4WT (gray bars, $4.73 \pm 1.64\%$, $n = 5$) and P2X4mCherryIN (red bars, $27.05 \pm 6.2\%$, $n = 3$). The number of independent experiments is indicated in parentheses, $*p < 0.05$, unpaired *t*-test. **e** Confocal overlay images of hippocampal neurons transfected with extracellular HA-tagged P2X4WT or HA-P2X4mCherryIN revealed a strong increase in surface P2X4 in neurons expressing P2X4mCherryIN vs. P2X4 WT. Surface P2X4 was revealed by labeling living cells with anti-HA antibodies (green). Total P2X4 was detected after fixation, permeabilization, and staining with anti-P2X4 antibody (red) in P2X4 WT cells or by mCherry fluorescence (red) in P2X4mCherryIN cells. Scale bars, 20 μ m. **f** Mean fluorescence intensity of surface HA-P2X4WT and HA-P2X4mCherryIN illustrated in **e** and in Supplementary Fig. S1. Error bars, s.e.m., the number of cells is indicated in parentheses, $***p < 0.001$, unpaired Mann-Whitney test. **g, h** Enlarged image of a dendrite, showing surface clustering of HA-P2X4mCherryIN. Postsynaptic regions are indicated by detection of Homer 1c (blue). Scale bar, 5 μ m. Overall, 42% of clusters are localized in the vicinity of excitatory glutamatergic synapses. **g** Quantification of the size, fluorescence intensity, and density of clusters at extrasynaptic site and in the vicinity of glutamatergic synapses showing P2X4 form larger clusters near synapses. Error bars: s.e.m., two-way ANOVA and Tukey's post hoc test, interaction $F(2, 341) = 11.38$; $***p < 0.001$. **i** Epifluorescence images of hippocampal neurons transfected with P2X4WT or P2X4mCherryIN revealed the strong increase of surface P2X4mCherryIN compared with P2X4WT. Surface P2X4WT and P2X4mCherryIN were revealed on living cells with Nodu-246 antibody (green) recognizing the native extracellular domain of P2X4. Total P2X4WT or P2X4mCherryIN was detected after fixation and permeabilization with anti-P2X4 antibodies (red) or directly by the red fluorescence of mCherry protein, respectively. Scale bar, 10 μ m.

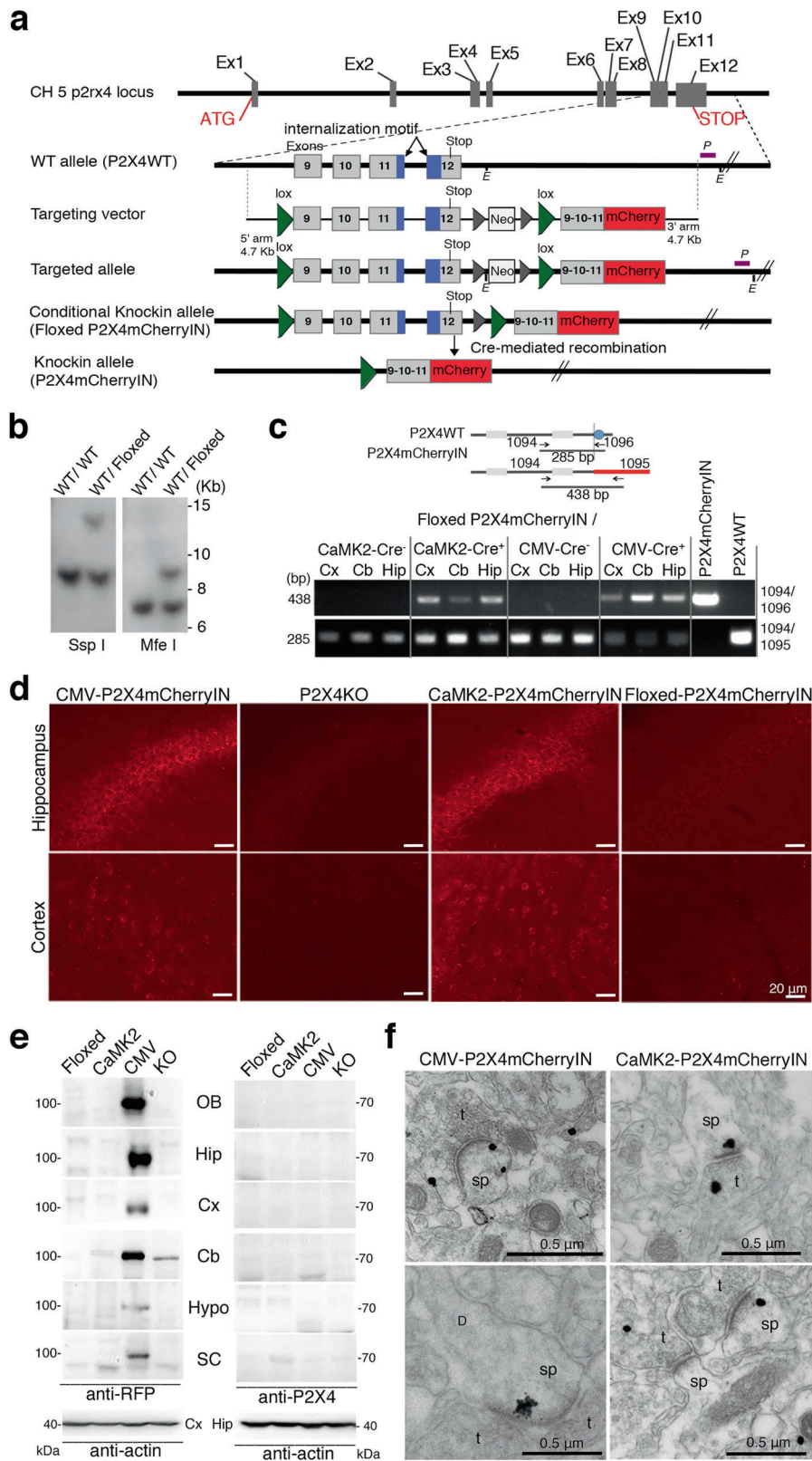
146 protein ratio showed that P2X4mCherryIN is more effectively
147 translocated to the surface than P2X4WT in *Xenopus*
148 oocytes (Fig. 1d, $p < 0.05$).

149 We next transfected hippocampal neurons and Cos cells
150 (Fig. 1e–h and Supplementary Fig. S1a–d) with extra-
151 cellularly tagged HA-P2X4WT and HA-P2X4mCherryIN
152 to visualize surface P2X4 on living cells using anti-HA

antibodies. Total HA-P2X4 was revealed after cell permeabilization using anti-P2X4 antibodies while the endogenous fluorescence of mCherry fused to P2X4 allowed for direct visualization. HA-P2X4WT is weakly expressed at the surface and is found mainly in intracellular puncta restricted to the soma and proximal dendrites of neurons [27]. In contrast, HA-P2X4mCherryIN was ~10 times more expressed at the surface of neurons. Surface P2X4mCherryIN puncta are uniformly distributed at the surface including distal dendrites. Co-staining with the postsynaptic marker Homer-1c-GFP revealed that surface P2X4mCherryIN are equally distributed in small extrasynaptic clusters and in larger clusters juxtaposed to synapses (Fig. 1g, h and Supplementary Fig. S1d). Finally, we confirmed the predominant intracellular localization of untagged P2X4WT in mouse transfected hippocampal neurons using Nodu-246, a rat monoclonal antibody recognizing the native extracellular domain of mouse P2X4 [52], whereas P2X4mCherryIN is highly and uniformly distributed at the cell surface (Fig. 1i).

172 Generation of knock-in mice with noninternalized 173 P2X4mCherryIN and expression in the brain

174 We generated the conditional Floxed P2X4mCherryIN
175 knock-in mice (Floxed) by homologous recombination
176 using a targeting vector (see Fig. 2a) designed to flox the
177 last four exons (exons 9 to 12) of *P2rx4* allele (P2X4
178 internalization motif being located on exons 11 and 12) and
179 followed by the insertion of a DNA fragment corresponding
180 to the fusion of exons 9, 10, and partially 11 with mCherry
181 cDNA. We next generated CMVCre⁺-P2X4mCherryIN^{F/F}
182 (namely CMV) mice and CaMK2Cre⁺-P2X4mCherryIN^{F/F}
183 (CaMK2) mice by breeding Floxed mice with mice either
184 expressing the Cre recombinase under the cytomegalovirus
185 (CMV-Cre) or the calmodulin kinase 2 (CaMK2-Cre) promoter
186 (Supplementary Fig. S2). Cre-dependent excision of
187 Floxed P2X4mCherryIN allele would lead to the replacement
188 of P2X4WT by noninternalized P2X4mCherryIN. It is
189 important to note that excised *p2rx4* gene remains under the
190 control of its own promoter, thus P2X4mCherryIN will
191 replace P2X4WT only in cells expressing natively P2X4
192 without altering its distribution pattern or its expression
193 level. In CMV mice, where a Cre-dependent excision
194 occurs in all cells, P2X4mCherryIN would replace
195 P2X4WT in all cells natively expressing P2X4 throughout
196 the body. In CaMK2 mice, substitution of P2X4WT by
197 P2X4mCherryIN is expected to be restricted to excitatory
198 forebrain neurons natively expressing P2X4, while other
199 P2X4 expressing cells such as glial cells and other neuronal
200 types express P2X4WT. Homozygous Floxed, CMV and
201 CaMK2 mice were used in all the following experiments
202 and were viable, normal in size or weight reproduced



203 normally and displayed no obvious physical or behavioral
204 abnormalities (see Supplementary information).

Reverse transcription (RT)-PCR in different brain 205
regions from the different mice showed that Floxed mice 206

◀ **Fig. 2 Generation of conditional P2X4mCherryIN knock-in mice and P2X4 expression in CMV-Cre or CaMK2-Cre P2X4mCherryIN knock-in mice.** **a** Schematic diagram of the mouse *P2xr4* gene and targeting vector strategy used to generate Floxed P2X4mCherryIN knock-in mice by homologous recombination (Floxed). By breeding Floxed P2X4mCherryIN with CMV-Cre mice or CaMK2-Cre mice, we generated constitutive CMVCre-P2X4mCherryIN (CMV) and CaMK2Cre-P2X4mCherryIN (CaMK2) to obtain a gain-of-function of P2X4 in all cells or in excitatory forebrain neurons natively expressing P2X4, respectively. **b** Southern blot of genomic DNA of WT and targeted allele (Floxed) using external probe (P) after digestion by *MfeI* or *SspI* enzyme (E) indicated in **a**. **c** Expression of P2X4WT and P2X4mCherryIN mRNAs by RT-PCR in cortex (Cx), cerebellum (Cb), and hippocampus (Hip) brain regions from Floxed P2X4mCherryIN, CMVCre⁺/Floxed P2X4mCherryIN (CMV) and CaMK2Cre⁺/Floxed P2X4mCherryIN (CaMK2) mice. **d–f** Protein expression of P2X4mCherryIN in the mouse brain revealed using anti-RFP antibodies recognizing mCherry protein. **d** Brain sections immunostained with anti-RFP antibodies show P2X4mCherryIN expression in the hippocampus and cortex of CMVCre-P2X4mCherryIN and CaMK2Cre-P2X4mCherryIN while no signal is visible in Floxed P2X4mCherryIN and P2X4 Knockout (KO) mice (see also Supplementary Fig. S3). Scale bar, 20 μ m. **e** Western blotting of total proteins extracted from distinct CNS regions isolated from CMV-P2X4mCherryIN (CMV), CaMK2-P2X4mCherryIN (CaMK2), Floxed P2X4mCherryIN, and P2X4KO mice revealed with anti-RFP or anti-P2X4 antibodies. Anti-tubulin antibody was used as a loading control. OB olfactory bulb, Hip hippocampus, Cx cortex, Cb cerebellum, Hypo hypothalamus, SC spinal cord. **f** Electron microscopy images showing preembedding anti-RFP immunostaining in CA1 region of the hippocampus or cortex from CMV-P2X4mCherryIN and CaMK2-P2X4mCherryIN mice (see also Supplementary Fig. S3). Staining is close to the plasma membrane of pre- and post-synaptic specializations of excitatory asymmetric synapses (top). Examples of spines where P2X4mCherryIN is detected only at the postsynapse, mainly located at the edge of the postsynaptic density. t presynaptic, sp spine. Scale bar, 0.5 μ m.

207 solely expressed P2X4WT mRNA while CMV mice only
 208 expressed P2X4mCherryIN mRNA (Fig. 2c). As expected,
 209 CaMK2 mice expressed both WT and knock-in mRNAs
 210 since only a subset of P2X4 expressing cells (forebrain
 211 excitatory neurons) replace P2X4WT by P2X4mCherryIN.
 212 Next, we tested P2X4mCherryIN expression in the brain on
 213 a protein level (Fig. 2d–f). The sparse expression of P2X4
 214 throughout the brain observed in previous works [3, 53]
 215 was recently confirmed using tdTomato *p2xr4* reporter mice in
 216 which the detection of cytosolic tdTomato-expressing cells
 217 required the use of anti-tdTomato antibodies [15]. Not
 218 surprisingly, endogenous fluorescence of mCherry fused to
 219 P2X4 was not directly visible on brain slices of the different
 220 knock-in mice but could be visualized using anti-RFP
 221 antibodies. P2X4mCherryIN was detected in the pyramidal
 222 neuron layer of the hippocampus and in the soma of neu-
 223 rons throughout the cortex [3, 15] in both CMV and
 224 CaMK2, but not in Floxed or P2X4 knockout (P2X4KO)
 225 mice (Fig. 2d). In addition, we confirmed the abundant
 226 expression of P2X4mCherryIN in the epithelial glomerular
 227 layer of the olfactory bulb [15, 54], as well as a moderate

228 presence in cerebellar Purkinje cells [3, 15] of CMV mice
 229 but not of CaMK2 mice, as expected. These results showed
 230 that P2X4mCherryIN distribution in CMV mice is similar to
 231 that of P2X4 in WT mice [15] and the restricted detection of
 232 P2X4mCherryIN in forebrain neurons in CaMK2 mice
 233 confirmed the specificity of Cre-dependent excision. (Sup-
 234 plementary Fig. S3a–b). The detection of a 100 kDa band
 235 with anti-RFP antibodies in western blots of total proteins
 236 from different brain regions confirmed the substitution of
 237 P2X4WT by P2X4mCherryIN in CMV mice (Fig. 2e). The
 238 absence of detection of P2X4mCherryIN in CaMK2 mice
 239 indicated that the replacement of P2X4WT by
 240 P2X4mCherryIN is more widespread in the CMV than in
 241 CaMK2 mice, as expected. Moreover, the absence of
 242 detection of P2X4WT in Floxed or CaMK2 mice with anti-
 243 P2X4 confirmed the sparse P2X4 expression in the brain
 244 tissues (Fig. 2e).

245 E.M. of anti-RFP labeling in hippocampal CA1 region or
 246 cortex revealed that P2X4mCherryIN was present at post-
 247 synaptic sites of excitatory synapses, preferentially at the
 248 edge of the postsynaptic density (Fig. 2f). At some asym-
 249 metric excitatory synapses, P2X4mCherryIN was located at
 250 both pre- and post-synaptic sites (Fig. 2f) and also found
 251 intracellularly in association with the endoplasmic reticulum
 252 membranes or occasionally with mitochondria (Supple-
 253 mentary Fig. S3c). This suggests that replacement of
 254 P2X4WT by P2X4mCherryIN does not alter its subcellular
 255 distribution [3]. The identification of symmetric synapses
 256 on morphological criteria being difficult, the presence of
 257 P2X4 at GABAergic synapses was not confirmed in CMV
 258 mice. In contrast, E.M. analysis revealed the presence of
 259 P2X4mCherryIN in astrocytes of CMV mice in the astro-
 260 cyte end-feet encircling endothelial cells (Supplementary
 261 Fig. S3d).

262 Endogenous P2X4mCherryIN fluorescence is directly 263 observable in macrophages or after LPS-induced de 264 novo expression in microglia of CMV mice

265 In mice, de novo P2X4 expression was observed in spinal
 266 microglia after nerve injury or in the brain after intracerebral
 267 lipopolysaccharide (LPS) injection in tdTomato *P2xr4*
 268 reporter mice [15, 38, 39, 41, 55]. We performed in vivo
 269 LPS microinjections into the hippocampus of CMV,
 270 CaMK2, Floxed, and P2X4KO mice and examined
 271 P2X4mCherryIN fluorescence (Fig. 3 and Supplementary
 272 Fig. S4). In control saline-injected mice, no endogenous
 273 mCherry fluorescence was visible in the hippocampus of all
 274 mouse genotypes and only a faint staining was revealed for
 275 the microglial marker Iba1 (Fig. 3a). In contrast, a strong
 276 increase in Iba1 staining was detected in all LPS-injected
 277 mouse lines attesting the microglial activation (Fig. 3a, b
 278 and Supplementary Fig. S4). Remarkably, endogenous

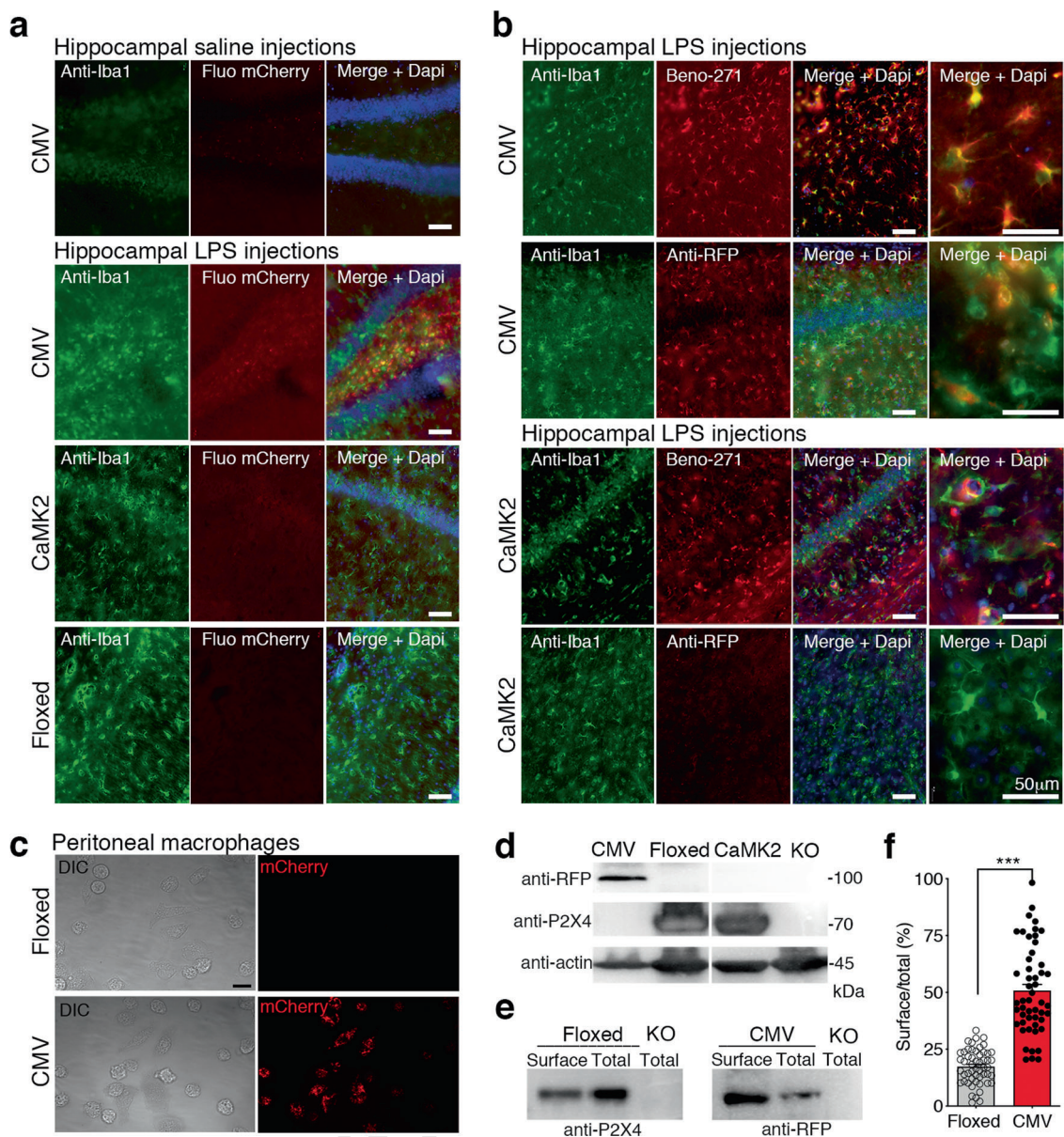


Fig. 3 Endogenous P2X4mCherryIN fluorescence in hippocampal microglia after LPS-induced de novo P2X4 expression and in peritoneal macrophages from CMV-P2X4mCherryIN mice. **a** Representative immunohistochemistry images of Iba1 and endogenous fluorescence of P2X4 mCherryIN (top, left) from the hippocampal region of the different mice injected with saline or 4 μ g LPS on each side (see also Supplementary Fig. S4). The mCherry fluorescence increased in Iba1-positive cells after LPS specifically in CMV mice. **b** Immunodetection of P2X4mCherryIN using Beno-271 antibodies (a camelid nanobody directed against the extracellular domain of native P2X4) and anti-RFP antibodies from CMV or CaMK2 mice after LPS injections. An enlarged overlay reveals that the increase of P2X4mCherryIN is detected in Iba1-positive microglia cells by both antibodies in CMV mice while such increase is observed only with Beno-271 in CaMK2 mice. Scale Bar, 50 μ m. **c** Endogenous P2X4mCherryIN fluorescence of macrophages isolated from the peritoneal cavity of Floxed and CMV mice. Differential interference contrast (DIC) and red fluorescence images reveal the P2X4mCherryIN exclusively in CMV mice. Scale bar, 20 μ m. **d** Western blotting

of total proteins from macrophages of CMV, CaMK2, Floxed, and P2X4KO mice using anti-RFP and anti-P2X4 revealed that P2X4WT is substituted by P2X4mCherryIN in macrophages of CMV mice only. P2X4mCherryIN is not detected by anti-P2X4 directed against the C-terminal of P2X4. Antiactin antibody was used as loading control. **e, f** Surface P2X4 expression is increased in CMV mouse peritoneal macrophages. Representative immunoblots of total and biotinylated surface proteins from peritoneal macrophages isolated from Floxed and CMV mice revealed with anti-P2X4 and anti-RFP antibodies, respectively. As in **d**, total proteins of P2X4KO macrophages were used as a negative control. **f** Quantification of surface/total expression of P2X4WT and P2X4mCherryIN in macrophages shown representatively in **e**. Bars represent mean \pm s.e.m. of the surface/total ratio of P2X4WT (Gray bar, $17.36 \pm 1.03\%$, $n = 53$) in Floxed mice and P2X4mCherryIN in CMV mice (red bar, $50.79 \pm 2.71\%$, $n = 51$) and show that P2X4 surface expression is strongly increased in cells expressing P2X4mCherryIN mice compared with those expressing P2X4WT. The number of independent experiments is indicated by clear and black circles. *** $P < 0.001$, unpaired t -test.

279 fluorescence of P2X4mCherryIN was directly visible and
 280 colocalized with Iba1 in CMV mice, but not in Floxed or
 281 CaMK2 mice. Anti-RFP confirmed the abundant and spe-
 282 cific P2X4mCherryIN expression in Iba1-positive cells
 283 solely in LPS-treated CMV mice. Notably, using Beno-271,
 284 a camelid nanobody recognizing the extracellular domain of
 285 mouse P2X4 [52], we showed increased P2X4 surface
 286 expression in microglia of CMV, CaMK2, and Floxed but
 287 not of P2X4KO mice (Fig. 3b and Supplementary Fig. S4).
 288 These results validate the cellular specificity of the Cre-
 289 mediated excision in both knock-in mice and show that de
 290 novo expression of P2X4 induced by LPS can be directly
 291 monitored by the visualization of the fluorescence of
 292 mCherry fused to P2X4.

293 P2X4 has been shown to be highly expressed in mac-
 294 rophages [41]. Endogenous mCherry fluorescence was
 295 directly visualized in freshly isolated peritoneal macro-
 296 phages from CMV mice (Fig. 3c), the only knock-in line
 297 expressing P2X4mCherryIN receptors in macrophages as
 298 confirmed by western blots of macrophages isolated from
 299 CMV, CaMK2, Floxed, and P2X4KO mice (Fig. 3d). To
 300 assess surface/total ratio of P2X4 and P2X4mCherryIN by
 301 western blot analysis, biotinylation assays were performed
 302 using macrophages in suspension. Our results showed that
 303 the number of surface P2X4mCherryIN is significantly
 304 higher in CMV (Fig. 3e, f) than in Floxed mice expressing
 305 P2X4WT, demonstrating that the substitution of P2X4 by
 306 P2X4mCherryIN leads to an increase in surface P2X4
 307 density in macrophages from CMV mice.

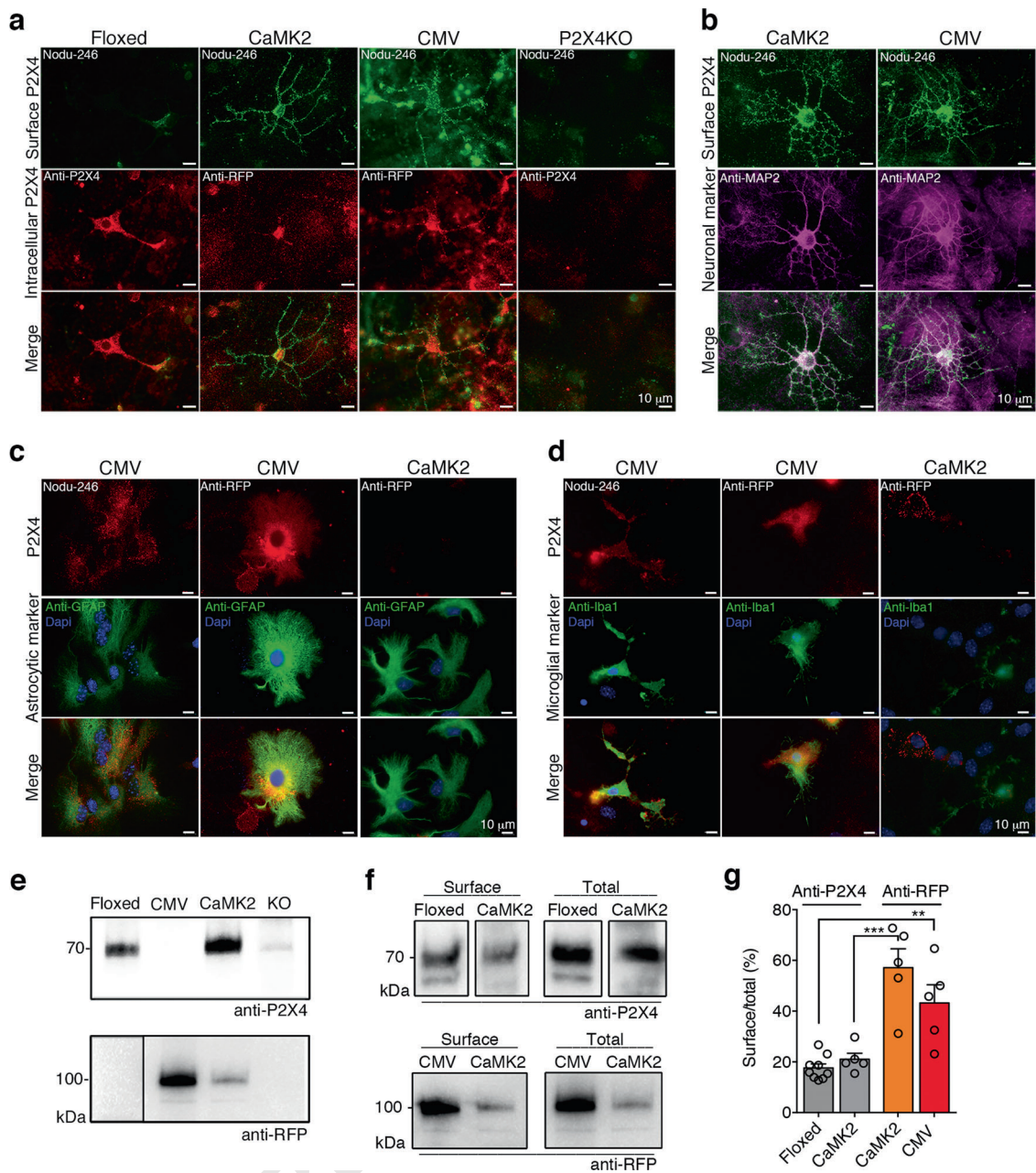
308 **P2X4mCherryIN is differentially upregulated at the** 309 **surface of neurons and glia in CMV and CaMK2 mice**

310 To demonstrate surface upregulation of P2X4mCherryIN in
 311 the CNS, we performed immunofluorescence experiments
 312 using hippocampal cultures from pups of both CMV,
 313 CaMK2 Floxed, or P2X4KO mice. We showed the distri-
 314 bution of surface vs. intracellular P2X4 using antibodies
 315 targeting either the native extracellular domain of P2X4
 316 (Nodu-246), or against the intracellular C-tail of either
 317 P2X4WT (anti-P2X4) or P2X4mCherryIN (anti-RFP,
 318 Fig. 4). In the Floxed mice, most P2X4WT was detected
 319 intracellularly (Fig. 4a) as described previously [27, 28, 34].
 320 In contrast, in both CMV and CaMK2 cells, a strong surface
 321 staining was detected using Nodu-246, as well as the pre-
 322 sence of RFP labeling, indicating the high density of
 323 P2X4mCherryIN on the surface of these hippocampal cells
 324 (Fig. 4a). In cells from P2X4KO mice, no P2X4 was
 325 detected on the cell surface or intracellular (Fig. 4a). Anti-
 326 MAP2 antibodies revealed the specific expression of
 327 P2X4mCherryIN in neurons in both CMV and CaMK2
 328 transgenic lines (Fig. 4b and Supplementary Fig. S5a).
 329 Using antibodies against astrocytic GFAP and microglial

330 Iba1 markers combined with Nodu-246 and anti-RFP,
 331 revealed the presence of surface P2X4mCherryIN in
 332 microglia and astrocytes from CMV, but not CaMK2 mice
 333 (Fig. 4c, d and Supplementary Fig. S5b). Consistently,
 334 western blotting of proteins extracted from hippocampal
 335 cultures of the different knock-in lines allowed the identi-
 336 fication of P2X4mCherryIN proteins in the CMV and
 337 CaMK2 exclusively, whereas P2X4WT was detected in
 338 Floxed and CaMK2 hippocampal cells (Fig. 4e). Next, we
 339 examined surface and total P2X4 levels using either anti-
 340 P2X4 or anti-RFP antibodies by biotinylation assays and
 341 western blotting of hippocampal cells from the different
 342 transgenic mice. Quantification of immunoblots (Fig. 4f)
 343 clearly indicates that P2X4WT in Floxed and CaMK2 mice
 344 is mainly intracellular (Fig. 4g), while the amount of
 345 P2X4mCherryIN on the cell surface is significantly higher
 346 in both CMV and CaMK2 cells (Fig. 4a–d). Altogether,
 347 these results confirm that substitution of P2X4WT by
 348 P2X4mCherryIN is restricted to excitatory neurons of
 349 CaMK2 mice while in CMV mice, the substitution occurs in
 350 all cells endogenously expressing P2X4 in CMV mice. In
 351 addition, our results demonstrate that P2X4mCherryIN
 352 expression leads to a stronger surface localization of
 353 P2X4mCherryIN in both CMV and CaMK2 mice (Fig. 4g).

354 **Increased surface density of P2X4 alters LTP and** 355 **LTD at CA1 hippocampal synapses**

356 We next examined the impact of noninternalized
 357 P2X4mCherryIN in hippocampal synaptic plasticity. Field
 358 excitatory postsynaptic potential (fEPSP) were recorded in
 359 the hippocampal CA1 region after stimulation of pre-
 360 synaptic Schaffer collateral axons in acute brain slices from
 361 control Floxed and both CaMK2 or CMV mice (Fig. 5a–f).
 362 The input/output curves obtained by plotting fEPSP slopes
 363 against the amplitude of stimulation (Fig. 5b) showed no
 364 significant differences between slices from CMV or CaMK2
 365 mice compared with control Floxed mice indicating that
 366 increased P2X4 surface receptors do not disrupt basal
 367 excitatory transmission at CA1 synapses. LTP and LTD
 368 were then evaluated. Robust LTP was induced in slices
 369 from Floxed mice with persistent potentiation (Fig. 5c, d).
 370 High frequency stimulation failed to trigger a potentiation in
 371 CaMK2 slices, while in CMV slices a potentiation was
 372 induced, but evoked responses returned rapidly to baseline
 373 after the induction. At 40 min post induction, LTP was
 374 absent in slices from both CMV and CaMK2 mice (Fig. 5c,
 375 d). Increased surface P2X4 appears to block LTD as well
 376 (Fig. 5e, f). LTD was induced in slices from Floxed, CMV
 377 and CaMK2 mice but a significant persistent synaptic
 378 depression was recorded solely in Floxed mice only
 379 (Fig. 5e, f). LTD from CMV and CaMK2 slices was not
 380 significantly different from baseline. Altogether, these



381 results demonstrate that increased surface P2X4 blocks LTP
 382 and alters LTD at hippocampal CA1 synapses. Moreover,
 383 the effects are more pronounced when surface P2X4 is
 384 increased exclusively in forebrain excitatory neurons.

385 **Increased surface density of P2X4 in forebrain**
 386 **neurons alters anxiety and memory functions**

387 Next, the impact of noninternalized P2X4mCherryIN
 388 expression on the behavior of the different transgenic mice
 389 was then examined using a battery of tests (Fig. 5g–p and
 390 Supplementary Fig. S6). First, potential changes in their
 391 general activity were assessed during open field exploration

(Fig. 5g–i). Floxed, CaMK2, and CMV mice showed 392
 similar velocity and total distance traveled in the arena, 393
 indicating that increased surface P2X4 does not modulate 394
 basal locomotor activity (Fig. 5g, h and Supplementary 395
 Fig. S6b). Interestingly, CaMK2 mice spent significantly 396
 more times in the central zone (red area) compared with the 397
 other groups of mice (Fig. 5i), suggesting that increased 398
 surface P2X4 density may reduce anxiety-like behavior. 399
 Neophobia-related anxiety was additionally examined by 400
 placing a novel object in the center of the arena (Fig. 5j–l; 401
 [56]). The latency to first exploring the novel object was 402
 slightly lower for CaMK2 than for CMV and Floxed mice 403
 but this difference failed to reach significance (Fig. 5k). 404

◀ **Fig. 4 Surface P2X4mCherryIN expression is increased in hippocampal neurons of CaMK2 or CMV mice as well as in glial cells of CMV mice.** **a** Representative images of surface and total P2X4WT and/or P2X4mCherryIN in Floxed, CMV, and CaMK2 primary hippocampal cell cultures reveal that surface P2X4mCherryIN is strongly increased compared with P2X4WT. Extracellular surface P2X4 and P2X4mCherryIN are visualized using Nodu-246 (green) antibodies. Intracellular P2X4WT is revealed by anti-P2X4 antibodies (red) in Floxed and P2X4KO mice while intracellular P2X4mCherryIN is revealed using anti-RFP antibodies (red) from CaMK2 and CMV mice. Staining was performed at 21 *div*. Scale bars, 10 μ m. **b** High density of surface P2X4mCherryIN using Nodu-246 (green) is detected in CaMK2 and CMV neurons identified using neuronal MAP2 marker (magenta). Surface P2X4WT is almost absent in Floxed mice and not detected in P2X4KO neurons (see Supplementary Fig. S5). **c, d** P2X4mCherryIN is expressed only in astrocytes and microglia of CMV mice solely. **c** Surface and total P2X4mCherryIN revealed using Nodu-246 and anti-RFP antibodies (red) respectively, in GFAP-positive astrocytes (green) from seven *div* primary hippocampal CMV cells. Nuclear marker DAPI is shown in blue. **d** Surface and total P2X4mCherryIN using Nodu-246 or anti-RFP antibodies (red), respectively, in microglia stained using anti-Iba1 antibodies (green) from 21 *div* primary hippocampal cells from CMV mice. Nuclear marker DAPI is shown in blue. **e** Western blotting of total proteins from primary hippocampal cells from Floxed, CMV, CaMK2, and P2X4KO mice using anti-RFP and anti-P2X4 antibodies reveal P2X4mCherryIN specifically in CMV and CaMK2 mice while P2X4WT is detected in CaMK2 and Floxed mice. **f** Representative immunoblots of total and biotinylated surface proteins from primary hippocampal cells isolated from Floxed, CMV, and CaMK2 mice revealed with either anti-P2X4, anti-RFP or both antibodies, respectively. As in **e**, total proteins of P2X4KO macrophages were used as a negative control. **g** Quantification of surface/total P2X4WT and P2X4mCherryIN in hippocampal cells. Bars represent mean \pm s.e.m. of the surface/total ratio of P2X4WT (gray bar) in Floxed and CaMK2 mice and P2X4mCherryIN in CaMK2 (orange bar) or CMV mice (red bar) and show that P2X4 surface expression is strongly increased in cells expressing P2X4mCherryIN mice compared with those expressing P2X4WT. The number of independent experiments is indicated by circles. one-way ANOVA, and Bonferroni's post hoc test, $F(3, 20) = 17.2$; * $p < 0.05$, ** $p < 0.01$, *** $p < 0.001$.

405 However, CaMK2 mice spent significantly more time
406 exploring the object than Floxed or CMV mice (Fig. 5l),
407 suggesting that anxiety is lower in these mice. To cor-
408 roborate these findings, the three mouse lines were tested in
409 the elevated plus maze (Fig. 5m). Compared with CMV and
410 Floxed mice, CaMK2 mice spent a greater proportion of
411 time in the open arms of the maze, confirming their
412 anxiolytic phenotype. These results indicate that neuronal
413 P2X4 is involved in the regulation of anxiety-like behavior,
414 with an increased number of P2X4 on neuronal surfaces
415 resulting in reduced anxiety.

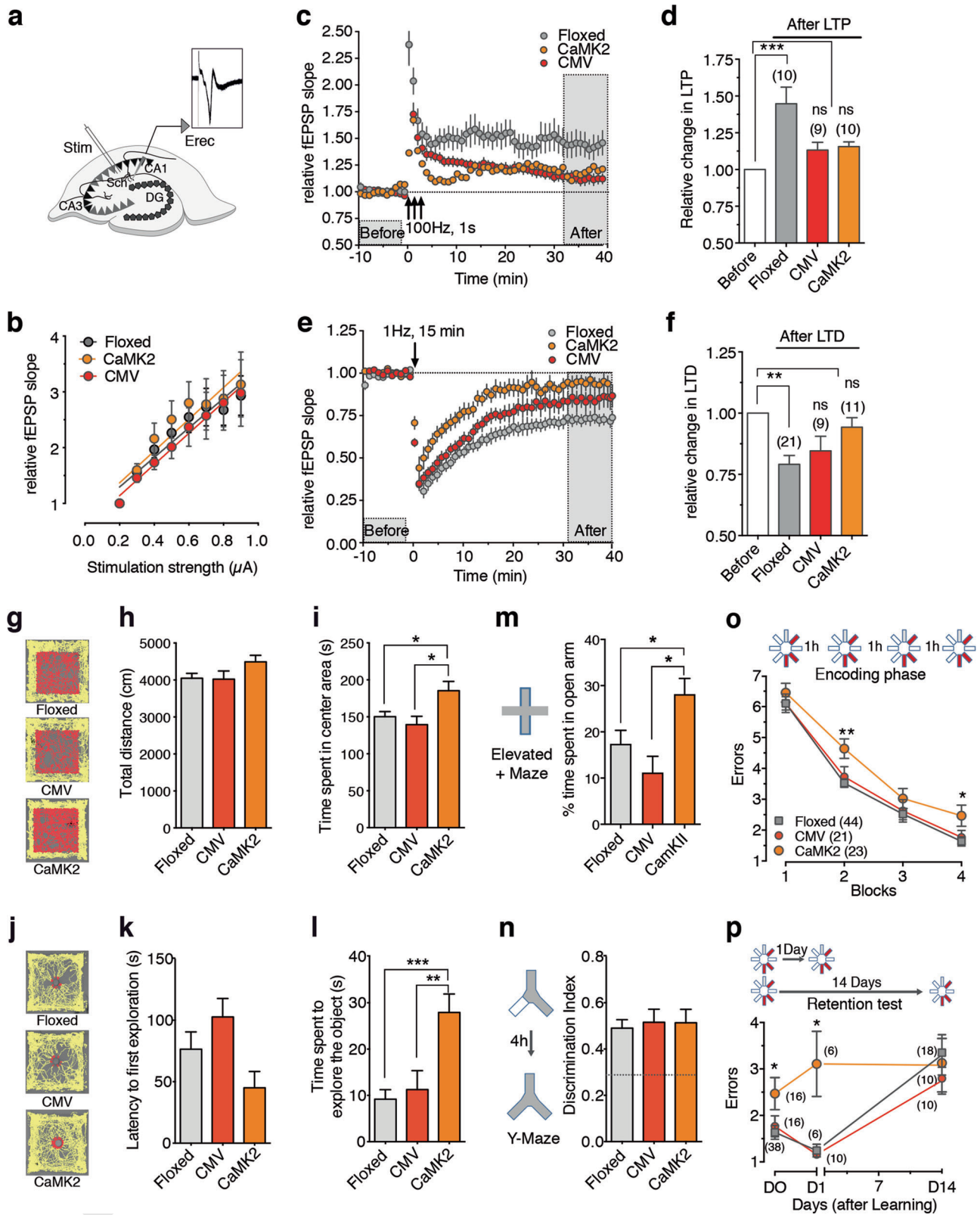
416 Spatial recognition memory was then evaluated using a
417 modified version of the Y-maze two-trial arm discrimina-
418 tion task (Fig. 5n and Supplementary Fig. S6; [57]). After a
419 single encoding phase of 10 min with only two accessible
420 arms, an inter-trial interval of 4 h resulted in a robust and
421 similar preference for the unexplored, previously inacces-
422 sible, arm during the test phase in CMV, CaMK2, and

Floxed mice. Thus, mice from all genotypes were capable
of processing visuo-spatial information and forming short-
term spatial recognition memory.

423
424
425
426 We next asked whether impairments in learning and
427 memory underlie the observed synaptic plasticity deficits.
428 We examined spatial memory in a more cognitively chal-
429 lenging situation by submitting CMV, CaMK2, and Floxed
430 mice to spatial discrimination tests in the eight-arm radial
431 maze. Mice were required to locate the three constantly
432 baited arms of the maze (Fig. 5o). To provide a rigorous
433 control over the time course of neuronal events induced by
434 spatial learning, we trained the mice over one single day.
435 Reference memory training consisted of four equivalent
436 blocks of six trials separated by a 1 h interval. Each trial
437 started with all eight arms opened and terminated when the
438 mouse entered the third baited arm and returned to the
439 central platform of the maze. While the number of reference
440 memory errors (i.e., entries into unbaited arms) decreased
441 significantly over the four training blocks in all three mouse
442 lines (Fig. 5o), CaMK2 mice made significantly more errors
443 than CMV and Floxed mice (Fig. 5k, $p = 0.0094$). Poorer
444 performance of CaMK2 was particularly apparent in train-
445 ing blocks 2 and 4 compared with Floxed and CMV mice.
446 Subsequently recent and long-term memory were evaluated
447 by submitting mice to retrieval testing 1 and 14 days after
448 training completion (Fig. 5p). As expected, Floxed mice
449 exhibited memory decay over time with an increased
450 number of reference memory errors at day 14. A similar
451 decay was observed in CMV mice, indicating that forgetting
452 was unaffected in this mouse line. In contrast, the poorer
453 performance of CaMK2 mice achieved upon training
454 remained stable across delays and was not further exacer-
455 bated by the passage of time. At day 14, the number of
456 reference memory errors was elevated but similar for all
457 three genotypes. Thus, selective expression of non-
458 internalized P2X4mCherryIN in excitatory forebrain neu-
459 rons translated into impaired spatial memory processing.

460 Discussion

461 To address pathologically increased surface P2X4 func-
462 tions, we created a Floxed knock-in P2X4mCherryIN
463 mouse line and generated two distinct conditional
464 P2X4mCherryIN lines, expressing noninternalized
465 P2X4mCherryIN either in all cells natively expressing
466 P2X4 (CMV mice) or in excitatory forebrain neurons
467 (CaMK2 mice), respectively. Both CMV and CaMK2
468 P2X4mCherryIN knock-in mice were viable, reproduced
469 normally and displayed no manifest phenotypic issues. The
470 key finding of this study is that the increased surface density
471 of P2X4 in forebrain excitatory neurons is a major regulator
472 of hippocampal synaptic plasticity, learning and memory



473 and anxiety functions indicating that increased neuronal
 474 P2X4 observed in AD models may have a key role in the
 475 pathogenesis of AD [25].

Importantly, analysis of P2X4mCherryIN expression
 showed that substitution of P2X4WT by P2X4mCherryIN
 occurred in the expected brain regions in both strains. In

476
 477
 478

Fig. 5 Surface increase of neuronal P2X4 impairs LTP and LTD at CA1 hippocampal synapses and alters anxiety, spatial learning, and memory. **a** Schematic drawing of the experimental protocol and example of an fEPSP recorded from the hippocampal CA1 region (Erec). fEPSP were induced by the electrical stimulation (stim) of the Schaffer collaterals (Sch) in the CA3 area and recorded in the stratum radiatum layer in brain slices of Floxed, CaMK2, and CMV P2X4mCherryIN mice. DG dentate gyrus. **b** The relative field slope is plotted against stimulation intensity. The input/output curves for neurons in hippocampal slices from Floxed (gray circles, $n = 7$), CaMK2 (orange circles, $n = 7$) and CMV P2X4mCherryIN (red circles, $n = 6$) mice show similar linear regression (mean \pm s.e.m., one-way ANOVA, $F(2, 18) = 0.15$; $p = 0.85$) indicating that basal synaptic transmission is not affected by the increase of surface P2X4 expression. **c, d** Surface P2X4 increase impairs LTP. **c** Plots of normalized fEPSP slopes recorded in CA1 over time before and after the induction of LTP. LTP was induced by three tetanic trains (100 Hz, 1 s) with a 20 sec interval) in control Floxed ($n = 10$), CaMK2 ($n = 10$) or CMV mice ($n = 9$). **d** Bar graph summary showing the relative change of fEPSP slope 30–40 min after the induction of LTP in Floxed ($144.7 \pm 11.3\%$ of baseline, $n = 10$), CMV mice ($113.2 \pm 5.27\%$ of baseline, $n = 9$) or CaMK2 ($115.6 \pm 3.25\%$ of baseline, $n = 10$), one-way ANOVA and tuckey's post hoc test; $F(3, 25) = 9.41$; $p = 0.002$, $***p < 0.001$. Error bars: s.e.m.; the number of mice is indicated in parentheses. **e, f** Increased surface P2X4 impairs LTD. **e** Plots of normalized fEPSP slopes recorded in CA1 over the time before and after the induction of LTD with a 1 Hz, 15 min train Floxed ($n = 21$), CaMK2 ($n = 11$), and CMV mice ($n = 9$). **f** Bar graph summary showing the relative change of fEPSP slope 30–40 min after the induction of LTD in Floxed ($79.09 \pm 3.63\%$ of the baseline, $n = 22$, $p < 0.001$), CMV ($84.58 \pm 5.97\%$ of baseline, $n = 8$, $p > 0.05$) and CaMK2 mice ($94.24 \pm 3.89\%$ of baseline, $n = 9$, $p > 0.05$). one-way ANOVA and tuckey's post hoc test; $F(3, 44) = 5.44$; $p = 0.0028$, $**p < 0.01$; Error bars: s.e.m.; the number of mice is indicated in parentheses. **g–i** Open field assessments of control (Floxed mice, $n = 24$) and CaMK2 ($n = 13$) or CMV ($n = 12$) P2X4mCherryIN mice. **g** Examples of exploration trajectories (top view) in the empty arena for each type of mice. Peripheral and central activities are indicated by yellow and red traces, respectively. **h** Similar total travel distance by

each mouse line in the empty arena during 10 min was similar. **i** CaMK2 mice spent more time in the central arena compared with Floxed and CMV mice, one-way ANOVA and Bonferroni's post hoc test; $F(2, 46) = 5.139$; $p = 0.0097$, $**p < 0.01$. **j–l** One object exploration test in control (Floxed mice, $n = 24$) and CaMK2 ($n = 13$) or CMV ($n = 12$) P2X4mCherryIN mice. **j** Examples of exploration trajectories (top view) for each type of mice. Activities far away or at proximity of the object are indicated in yellow or red, respectively. **k** Latency to first interaction with the novel object is shown for each type of mouse. One-way ANOVA and Bonferroni's post hoc test, $F(2, 46) = 2.868$; $p = 0.067$. **l** CaMK2 mice spent more time exploring the novel object than Floxed and CMV mice. One-way ANOVA, $F(2, 46) = 10.27$; $p = 0.0002$; $**p < 0.01$, $***p < 0.001$. **m** Mean percent of time spent in the open arms of the elevated plus maze for Floxed mice ($n = 22$), CaMK2 ($n = 14$), and CMV ($n = 11$) mice. CaMK2 spent more time in the open arms, indicating reduced anxiety compared with the other mouse lines. One-way ANOVA and Bonferroni's post hoc test, $F(2, 44) = 5.186$; $p = 0.0095$; $*p < 0.05$. **n** Spatial recognition memory evaluated in the Y-maze. Floxed ($n = 24$), CaMK2 ($n = 13$), or CMV ($n = 12$) mice were able to recognize the novel arm of the maze that was rendered accessible 4 h after encoding (one-way ANOVA, $F(2, 46) = 0.097$; $p = 0.907$). **o, p** Spatial learning and memory assessment using the eight-radial maze in Floxed mice (gray), CaMK2 (orange) and CMV (red) mice. The number of mice in each group is indicated in parentheses. **o** Learning occurred over one single day and consisted of four blocks of six trials separated by a 1 h interval. The location of the three constantly baited arms of the maze is indicated in red. CaMK2 mice committed more reference memory errors (visits to unbaited arms) compared with Floxed and CMV mice. $*p < 0.05$, $**p < 0.01$. Paired two-way ANOVA and Bonferroni's post hoc test, Time effect, $F(3, 255) = 205.3$, $p < 0.0001$. Paired two-way ANOVA, genotype effect, $F(2, 85) = 4927$, $p = 0.0094$. **p** Retrieval testing 1 (recent) or 14 (long-term) days after initial training in the eight-arm radial maze for all three mouse lines. Performance achieved on the fourth training block (D0) is shown for comparison. The poorer performance exhibited by CaMK2 mice (higher number of errors) was not exacerbated by the passage of time. $*p < 0.05$, paired two-way ANOVA and Bonferroni's post hoc test, delay effect, $F(1, 35) = 11.70$; $p = 0.0016$. All data are presented as mean \pm s.e.m.

479 CMV mice, the expression pattern of P2X4mCherryIN is
480 consistent with what was described for WT P2X4 in the
481 CNS, i.e., high expression in the olfactory epithelium and a
482 sparse expression in the hippocampus, cortex, cerebellum,
483 and spinal cord [3, 15, 53]. In addition, and in line with
484 other findings [41, 58], P2X4mCherryIN was also found
485 expressed in peritoneal macrophages of CMV mice. In
486 CaMK2 mice, P2X4mCherryIN expression was mainly
487 restricted to hippocampal and cortical regions, in line with
488 previous reports of CaMK2 promoter selectivity [59]. The
489 in vitro expression of P2X4mCherryIN construct revealed
490 that the substitution of the last 11 amino acids of the C-tail
491 of mouse P2X4 by the red fluorescent protein mCherry
492 increases surface trafficking without altering P2X4 function
493 and subcellular targeting [3, 27, 28, 30, 42, 43]. Indeed, in
494 both CMV and CaMK2 knock-in mice, E.M. confirmed that
495 P2X4mCherryIN are localized at both pre- and post-
496 synaptic specializations in hippocampal or cortical excita-
497 tory neurons, as expected [2, 3, 15]. Inhibitory symmetric
498 synapses are difficult to identify based on morphology

499 criteria, thus the presence of P2X4mCherryIN at the
500 GABAergic synapse, where P2X4 was reported to be pre-
501 sent, remains to be shown by including specific markers
502 [9, 10, 42]. Surface and intracellular staining on hippo-
503 campal cultures as well as biotinylation experiments from
504 the different knock-in mice demonstrate that substitution of
505 P2X4WT by P2X4mCherryIN induced a significant
506 increase in surface P2X4 in both CaMK2 and CMV neu-
507 rons. In addition, P2X4mCherryIN was found to be present
508 and upregulated at the surface of hippocampal microglia
509 and astrocytes as well as macrophages of CMV mice. P2X4
510 expression in astrocytes has been previously observed, but
511 was debated [60]. Notably, P2X4mCherryIN was detected
512 in hippocampal astrocytes in vitro, but was detected on
513 brain slices by E.M. only.

514 In contrast to transfected cells overexpressing
515 P2X4mCherryIN, direct fluorescence of P2X4mCherryIN
516 was undetectable from brain slices and hippocampal cul-
517 tures of both knock-in mice, preventing the direct identifi-
518 cation and functional characterization of P2X4mCherryIN-

519 expressing cells. Fluorescence of P2X4mCherryIN was
520 directly visible solely in isolated peritoneal macrophages of
521 CMV mice in agreement with its high basal expression in
522 macrophages [41]. Interestingly, following LPS injection in
523 the hippocampus to induce microglial activation and
524 increase de novo P2X4 expression [15], endogenous
525 fluorescence of P2X4mCherryIN was revealed in Iba1-
526 positive microglia exclusively in CMV mice. These results
527 indicate that the P2X4mCherryIN fluorescence may repre-
528 sent a unique tool to directly monitor increased P2X4
529 expression in pathological models such as chronic pain,
530 AD, ALS, alcohol intake, inflammation, epilepsy, ischemia,
531 or brain trauma [14, 19, 22, 23, 25, 26, 35–38, 55, 61].

532 LTP and LTD phenomena are widely recognized as
533 crucial molecular mechanisms underlying cognitive func-
534 tions such as learning and memory [62]. Although activa-
535 tion of P2X receptors by glial ATP was recently shown to
536 directly modulate glutamatergic synaptic strength [10], P2X
537 receptors exert modulatory actions exclusively during
538 activity-dependent plasticity at central synapses and do not
539 influence basal synaptic transmission [17, 18, 63]. Previous
540 studies have shown P2X4 modulating hippocampal LTP via
541 N-methyl-D-aspartate receptor receptors (NMDAR), how-
542 ever these findings remained controversial. The first work
543 using P2X4KO mice revealed that LTP in CA1 neurons was
544 slightly reduced compared with WT mice and that potentia-
545 tion of P2X4 by ivermectin enhanced LTP only in WT
546 mice [17]. Results suggested that P2X4 may enhance the
547 content of NR2B subunits in synaptic NMDARs [63]. In
548 contrast, an other study showed that the pharmacological
549 blockade of P2X4 facilitated the induction of NMDAR-
550 dependent LTP indicating an inhibitory impact of P2X4
551 [18, 64]. Furthermore, increased P2X4 expression was
552 reported in AD models [25] suggesting that P2X4 might
553 also contribute to synaptic dysfunction and memory deficits.
554 Field potential recordings show that P2X4mCherryIN
555 expression does not change the basal excitatory transmis-
556 sion at CA1 synapses but causes impairments in both LTP
557 and LTD in agreement with a negative impact of P2X4 on
558 synaptic plasticity. Surprisingly, but in full agreement with
559 our behavioral results, these deficits were stronger in
560 CaMK2 than in CMV mice. Impaired LTP observed in
561 CaMK2 mice occurred immediately suggesting a deficit of
562 LTP induction. In contrast, in CMV mice, LTP was induced
563 but progressively returned to baseline, rather indicating a
564 deficit in LTP maintenance. Since basal excitation mediated
565 by α -amino-3-hydroxy-5-methyl-4-isoxazolepropionic acid
566 receptor (AMPA) is unchanged, and LTD or LTP in
567 hippocampal CA1 neurons are mainly initiated post
568 synaptically by NMDAR [62], our results suggest that
569 increased P2X4 in CA1 neurons might alter NMDAR
570 function. P2X4 is highly permeable to calcium and can
571 mediate a strong calcium influx at the resting membrane

572 potential that may induce NMDAR inactivation [64]. P2X4
573 interacts also dynamically with various other ligand-gated
574 ion channels such as GABA_A [10, 42, 65] and may lead to
575 NMDAR inhibition by similar crosstalk.

576 Behavioral phenotyping of the CMV mice did not reveal
577 any overt alterations. In contrast, CaMK2 mice exhibited a
578 significant decrease in anxiety-like behaviors and impaired
579 spatial learning and memory functions. No change in
580 locomotor, anxiety-like or cognitive functions were pre-
581 viously observed in P2X4KO mice [66]. Together, these
582 results suggest that, in contrast to the basal state, increased
583 surface P2X4 density observed in neurons in pathological
584 situations such as in AD [25] might play essential roles in
585 the regulation of synaptic plasticity and behavior such as
586 anxiety and learning and memory.

587 The absence of a phenotype of the CMV mice, although
588 in agreement with the weaker effects on the synaptic plas-
589 ticity of CMV compared with CaMK2 mice, is intriguing
590 since substitution of P2X4WT by P2X4mCherryIN in all
591 cells natively expressing P2X4 was expected to have more
592 pronounced effects than specific P2X4mCherryIN expres-
593 sion solely in forebrain excitatory neurons. However, this
594 could be explained by temporal differences between CMV
595 and CaMK2 promoter activation. CMV is a ubiquitous early
596 gene promoter leading to the genetic excision of Floxed
597 P2X4mCherryIN in the germ-line and consequently from
598 the beginning of the embryonic development while the
599 CaMK2 promoter is considered as an adult promoter with
600 postnatal activity reaching its maximum around the third
601 postnatal week [67]. Expression of P2X4mCherryIN in all
602 cells natively expressing P2X4 during the developmental
603 period and thereafter may have deleterious effects leading to
604 developmental compensations. Another possibility is that
605 the expression of P2X4mCherryIN in CMV mice in other
606 types of neurons along with expression in glial cells may
607 counterbalance the effect of its increased surface density
608 specifically in excitatory neurons. Indeed, increased P2X4
609 expression in spinal cord microglia during neuropathic
610 conditions triggers the release of BDNF by microglia
611 resulting in neuronal hyperexcitability [39, 40]. In addition,
612 microglia and BDNF have been shown to influence synaptic
613 plasticity and learning in the brain [68]. These results sug-
614 gest that increased surface P2X4 in microglia of CMV mice
615 may promote synaptic plasticity and counterbalance the
616 negative impact of an increase of surface P2X4 specifically
617 in excitatory neurons of CaMK2 mice.

618 P2X4 is present in multiple cell types in the peripheral or
619 CNS and in various epithelial, endothelial, or immune cells.
620 After injury and during inflammation and cell damage, high
621 levels of ATP are released and P2X4 is strongly upregulated
622 on cell surfaces. This upregulation seems to orchestrate key
623 events during neurodegenerative diseases, neuropathic and
624 inflammatory pain, ischemia-induced inflammation, alcohol

625 intake, airways inflammation in asthma, rheumatoid arthritis
626 or postsurgical liver regeneration (see for review [14]).

627 These novel conditional knock-in mice defective for
628 P2X4 internalization provide a valuable tool which will
629 allow to further decipher the role of upregulated P2X4 state
630 not only in the context of neurological diseases, but also of
631 peripheral inflammation, infection as well as in lung, car-
632 diac or liver functions [69–73].

633 **Acknowledgements** We thank G. Dabee for the production of all
634 transgenic mice at the animal facility, H. Orignac for help with
635 *Xenopus* facilities and E. Normand for stereotaxic injection. We thank
636 the Mouse Clinical Institute (Institut Clinique de la Souris, MCI/ICS)
637 in the Genetic Engineering and Model Validation Department who
638 established the mouse mutant floxed P2X4mCherryIN line. We also
639 thank the biochemistry facility of Bordeaux Neurocampus. Electron
640 microscopy was performed at the Bordeaux Imaging Center, a service
641 unit of the CNRS-INSERM and Bordeaux University. This work was
642 supported by CNRS, University of Bordeaux, a grant LabEx BRAIN
643 ANR-10-LABX-43 to EB-G and EB, a grant from Inserm for the
644 generation of the mouse line to EB-G, the Louise and Alan Edwards
645 Foundation, an awarded grant from Quebec Pain Research Network
646 (QPRN) to TD, International Ph. D program of the IdEx of Bordeaux
647 to EB-G and PS and DFG grant SFB1328-Z02 to FK-N.

648 **Author contributions** EB, TD, KSP, AM, J-TP, ED, A-EA, ET, MR,
649 FG, ON performed the experiments and analyzed the data. PS, BB, SL,
650 FG, SB, ON and EB-G designed the experiments and analyzed the
651 data. PB, EB, FK-N contributed with key reagents. EB-G conceived
652 the knock-in mice and the study. KSP, ON, and EB-G wrote the paper.
653 All authors commented the paper.

654 Compliance with ethical standards

655 **Conflict of interest** The authors declare they have no conflict of
656 interest.

657 **Ethical approval** All experimental procedures complied with official
658 European guidelines for the care and use of laboratory animals
659 (Directive 2010/63/UE).

660 **Publisher's note** Springer Nature remains neutral with regard to
661 jurisdictional claims in published maps and institutional affiliations.

662 References

- 663 1. Khakh BS, North RA. Neuromodulation by extracellular ATP and
664 P2X receptors in the CNS. *Neuron*. 2012;76:51–69.
- 665 2. Rodrigues RJ, Almeida T, Richardson PJ, Oliveira CR, Cunha
666 RA. Dual presynaptic control by ATP of glutamate release via
667 facilitatory P2X1, P2X2/3, and P2X3 and inhibitory P2Y1, P2Y2,
668 and/or P2Y4 receptors in the rat hippocampus. *J Neurosci*.
669 2005;25:6286–95.
- 670 3. Rubio ME, Soto F. Distinct localization of P2X receptors at exci-
671 tatory postsynaptic specializations. *J Neurosci*. 2001;21:641–53.
- 672 4. Kaczmarek-Hajek K, Zhang J, Kopp R, Grosche A, Rissiek B,
673 Saul A, et al. Re-evaluation of neuronal P2X7 expression using
674 novel mouse models and a P2X7-specific nanobody. *eLife*.
675 2018;7:e36217.
- 676 5. Jo YH, Schlichter R. Synaptic corelease of ATP and GABA in
677 cultured spinal neurons. *Nat Neurosci*. 1999;2:241–5.

- 678 6. Mori M, Heuss C, Gahwiler BH, Gerber U. Fast synaptic trans-
679 mission mediated by P2X receptors in CA3 pyramidal cells of rat
680 hippocampal slice cultures. *J Physiol*. 2001;535:115–23.
- 681 7. Gordon GR, Baimoukhametova DV, Hewitt SA, Rajapaksha WR,
682 Fisher TE, Bains JS. Norepinephrine triggers release of glial ATP
683 to increase postsynaptic efficacy. *Nat Neurosci*. 2005;8:1078–86.
- 684 8. Pougnet JT, Toulme E, Martinez A, Choquet D, Hosy E, Boue-
685 Grabot E. ATP P2X receptors downregulate AMPA receptor
686 trafficking and postsynaptic efficacy in hippocampal neurons.
687 *Neuron*. 2014;83:417–30.
- 688 9. Lalo U, Palygin O, Rasooli-Nejad S, Andrew J, Haydon PG,
689 Pankratov Y. Exocytosis of ATP from astrocytes modulates
690 phasic and tonic inhibition in the neocortex. *PLoS Biol*. 2014;12:
691 e1001747.
- 692 10. Boué-Grabot E, Pankratov Y. Modulation of central synapses by
693 astrocyte-released ATP and postsynaptic P2X receptors. *Neural
694 Plast*. 2017;2017:9454275.
- 695 11. Illes P, Verkhratsky A. Purinergic neurone-glia signalling in
696 cognitive-related pathologies. *Neuropharmacology*. 2016;104:62–75.
- 697 12. Kawate T, Michel JC, Birdsong WT, Gouaux E. Crystal structure
698 of the ATP-gated P2X(4) ion channel in the closed state. *Nature*.
699 2009;460:592–8.
- 700 13. Egan TM, Khakh BS. Contribution of calcium ions to P2X
701 channel responses. *J Neurosci*. 2004;24:3413–20.
- 702 14. Suurväli J, Boudinot P, Kanellopoulos J, Rüttel Boudinot S.
703 P2X4: a fast and sensitive purinergic receptor. *Biomed J*.
704 2017;40:245–56.
- 705 15. Xu J, Bernstein AM, Wong A, Lu XH, Khoja S, Yang XW, et al.
706 P2X4 receptor reporter mice: sparse brain expression and feeding-
707 related presynaptic facilitation in the arcuate nucleus. *J Neurosci*.
708 2016;36:8902–20.
- 709 16. Yeung D, Kharidia R, Brown SC, Gorecki DC. Enhanced expres-
710 sion of the P2X4 receptor in Duchenne muscular dystrophy corre-
711 lates with macrophage invasion. *Neurobiol Dis*. 2004;15:212–20.
- 712 17. Sim JA, Chaumont S, Jo J, Ulmann L, Young MT, Cho K, et al.
713 Altered hippocampal synaptic potentiation in P2X4 knock-out
714 mice. *J Neurosci*. 2006;26:9006–9.
- 715 18. Pankratov Y, Lalo U, Krishtal OA, Verkhratsky A P2X receptors
716 and synaptic plasticity. *Neuroscience*. 2008.
- 717 19. Cavaliere F, Florenzano F, Amadio S, Fusco FR, Viscomi MT,
718 D'Ambrosi N, et al. Up-regulation of P2X2, P2X4 receptor and
719 ischemic cell death: prevention by P2 antagonists. *Neuroscience*.
720 2003;120:85–98.
- 721 20. Franke H, Illes P. Involvement of P2 receptors in the growth and
722 survival of neurons in the CNS. *Pharm Ther*. 2006;109:297–324.
- 723 21. Burnstock G. Purinergic signalling and disorders of the central
724 nervous system. *Nat Rev Drug Disco*. 2008;7:575–90.
- 725 22. Apolloni S, Montilli C, Finocchi P, Amadio S. Membrane com-
726 partments and purinergic signalling: P2X receptors in neurodegen-
727 erative and neuroinflammatory events. *FEBS J*. 2009;276:354–64.
- 728 23. Volonte C, Apolloni S, Parisi C, Amadio S. Purinergic contribu-
729 tion to amyotrophic lateral sclerosis. *Neuropharmacology*. 2016;
730 104:180–93.
- 731 24. Beggs S, Trang T, Salter MW. P2X4R+ microglia drive neuro-
732 pathic pain. *Nat Neurosci*. 2012;15:1068–73.
- 733 25. Varma R, Chai Y, Troncoso J, Gu J, Xing H, Stojilkovic SS, et al.
734 Amyloid-beta induces a caspase-mediated cleavage of P2X4 to
735 promote purinotoxicity. *Neuromolecular Med*. 2009;11:63–75.
- 736 26. Casanovas A, Hernandez S, Tarabal O, Rossello J, Esquerda JE.
737 Strong P2X4 purinergic receptor-like immunoreactivity is selec-
738 tively associated with degenerating neurons in transgenic rodent
739 models of amyotrophic lateral sclerosis. *J Comp Neurol*.
740 2008;506:75–92.
- 741 27. Bobanovic LK, Royle SJ, Murrell-Lagnado RD. P2X receptor
742 trafficking in neurons is subunit specific. *J Neurosci*. 2002;
743 22:4814–24.

- 744 28. Royle SJ, Bobanovic LK, Murrell-Lagnado RD. Identification of a
745 non-canonical tyrosine-based endocytic motif in an ionotropic
746 receptor. *J Biol Chem.* 2002;277:35378–85.
- 747 29. Qureshi OS, Paramasivam A, Yu JC, Murrell-Lagnado RD.
748 Regulation of P2X4 receptors by lysosomal targeting, glycan
749 protection and exocytosis. *J Cell Sci.* 2007;120:3838–49.
- 750 30. Royle SJ, Qureshi OS, Bobanovic LK, Evans PR, Owen DJ,
751 Murrell-Lagnado RD. Non-canonical YXXGPhi endocytic motifs:
752 recognition by AP2 and preferential utilization in P2X4 receptors.
753 *J Cell Sci.* 2005;118:3073–80.
- 754 31. Toulme E, Garcia A, Samways D, Egan TM, Carson MJ, Khakh
755 BS. P2X4 receptors in activated C8-B4 cells of cerebellar
756 microglial origin. *J Gen Physiol.* 2010;135:333–53.
- 757 32. Cao Q, Zhong XZ, Zou Y, Murrell-Lagnado R, Zhu MX, Dong XP.
758 Calcium release through P2X4 activates calmodulin to promote
759 endolysosomal membrane fusion. *J Cell Biol.* 2015;209:879–94.
- 760 33. Huang P, Zou Y, Zhong XZ, Cao Q, Zhao K, Zhu MX, et al.
761 P2X4 forms functional ATP-activated cation channels on lyso-
762 somal membranes regulated by luminal pH. *J Biol Chem.*
763 2014;289:17658–67.
- 764 34. Robinson LE, Murrell-Lagnado RD. The trafficking and targeting
765 of P2X receptors. *Front Cell Neurosci.* 2013;7:233.
- 766 35. Andries M, Van Damme P, Robberecht W, Van Den Bosch L.
767 Ivermectin inhibits AMPA receptor-mediated excitotoxicity in
768 cultured motor neurons and extends the life span of a transgenic
769 mouse model of amyotrophic lateral sclerosis. *Neurobiol Dis.*
770 2007;25:8–16.
- 771 36. Khoja S, Huynh N, Asatryan L, Jakowec MW, Davies DL.
772 Reduced expression of purinergic P2X4 receptors increases
773 voluntary ethanol intake in C57BL/6J mice. *Alcohol.* 2018;
774 68:63–70.
- 775 37. Wyatt LR, Finn DA, Khoja S, Yardley MM, Asatryan L, Alkana
776 RL, et al. Contribution of P2X4 receptors to ethanol intake in male
777 C57BL/6 mice. *Neurochem Res.* 2014;39:1127–39.
- 778 38. Tsuda M, Shigemoto-Mogami Y, Koizumi S, Mizokoshi A,
779 Kohsaka S, Salter MW, et al. P2X4 receptors induced in spinal
780 microglia gate tactile allodynia after nerve injury. *Nature.*
781 2003;424:778–83.
- 782 39. Ulmann L, Hatcher JP, Hughes JP, Chaumont S, Green PJ,
783 Conquet F, et al. Up-regulation of P2X4 receptors in spinal
784 microglia after peripheral nerve injury mediates BDNF release and
785 neuropathic pain. *J Neurosci.* 2008;28:11263–8.
- 786 40. Coull JA, Beggs S, Boudreau D, Boivin D, Tsuda M, Inoue K,
787 et al. BDNF from microglia causes the shift in neuronal anion
788 gradient underlying neuropathic pain. *Nature.* 2005;438:1017–21.
- 789 41. Ulmann L, Hirbec H, Rassendren F. P2X4 receptors mediate
790 PGE2 release by tissue-resident macrophages and initiate
791 inflammatory pain. *EMBO J.* 2010;29:2290–300.
- 792 42. Jo YH, Donier E, Martinez A, Garret M, Toulme E, Boue-Grabot
793 E. Cross-talk between P2X4 and gamma-aminobutyric acid, type
794 A receptors determines synaptic efficacy at a central synapse. *J
795 Biol Chem.* 2011;286:19993–20004.
- 796 43. Toulme E, Soto F, Garret M, Boue-Grabot E. Functional prop-
797 erties of internalization-deficient P2X4 receptors reveal a novel
798 mechanism of ligand-gated channel facilitation by ivermectin.
799 *Mol Pharm.* 2006;69:576–87.
- 800 44. Chamma I, Heubl M, Chevy Q, Renner M, Moutkine I, Eugene E,
801 et al. Activity-dependent regulation of the K/Cl transporter KCC2
802 membrane diffusion, clustering, and function in hippocampal
803 neurons. *J Neurosci.* 2013;33:15488–503.
- 804 45. Ray A, Dittel BN. Isolation of mouse peritoneal cavity cells. *J Vis
805 Exp.* 2010.
- 806 46. Berthet A, Porras G, Doudnikoff E, Stark H, Cador M, Bezard E,
807 et al. Pharmacological analysis demonstrates dramatic alteration of
808 D1 dopamine receptor neuronal distribution in the rat analog of L-
809 DOPA-induced dyskinesia. *J Neurosci.* 2009;29:4829–35.
47. Bertin E, Martinez A, Boue-Grabot E. P2X Electrophysiology and
810 Surface Trafficking in *Xenopus* Oocytes. *Methods Mol Biol.*
811 2020;2041:243–59.
48. Belzung C. Hippocampal mossy fibres: implication in novelty
812 reactions or in anxiety behaviours? *Behav Brain Res.* 1992;
813 51:149–55.
49. Renner MJ, Bennett AJ, White JC. Age and sex as factors influ-
814 encing spontaneous exploration and object investigation by pre-
815 adult rats (*Rattus norvegicus*). *J Comp Psychol.* 1992;106:217–27.
50. Pellow S, File SE. Anxiolytic and anxiogenic drug effects on
816 exploratory activity in an elevated plus-maze: a novel test of
817 anxiety in the rat. *Pharm Biochem Behav.* 1986;24:525–9.
51. Dellu F, Contarino A, Simon H, Koob GF, Gold LH. Genetic
818 differences in response to novelty and spatial memory using a
819 two-trial recognition task in mice. *Neurobiol Learn Mem.*
820 2000;73:31–48.
52. Bergmann P, Garcia de Paco A, Rissiek B, Menzel S, Dubberke
821 G, Hua J et al. Generation and characterization of specific
822 monoclonal antibodies and Nanobodies directed against the ATP-
823 gated channel P2X4. *Front Cell Neurosci.* in press.
53. Lê KT, Villeneuve P, Ramjaun AR, McPherson PS, Beaudet A,
824 Seguela P. Sensory presynaptic and widespread somatodendritic
825 immunolocalization of central ionotropic P2X ATP receptors.
826 *Neuroscience.* 1998;83:177–90.
54. Buell G, Lewis C, Collo G, North RA, Surprenant A. An
827 antagonist-insensitive P2X receptor expressed in epithelia and
828 brain. *EMBO J.* 1996;15:55–62.
55. Ulmann L, Levavasseur F, Avignone E, Peyrourou R, Hirbec H,
829 Audinat E, et al. Involvement of P2X4 receptors in hippocampal
830 microglial activation after status epilepticus. *Glia.* 2013;
831 61:1306–19.
56. Dulawa SC, Grandy DK, Low MJ, Paulus MP, Geyer MA.
832 Dopamine D4 receptor-knock-out mice exhibit reduced explora-
833 tion of novel stimuli. *J Neurosci.* 1999;19:9550–6.
57. Nicole O, Hadzibegovic S, Gajda J, Bontempi B, Bem T, Meyr-
834 and P. Soluble amyloid beta oligomers block the learning-induced
835 increase in hippocampal sharp wave-ripple rate and impair spatial
836 memory formation. *Sci Rep.* 2016;6:22728.
58. Layhadi JA, Turner J, Crossman D, Fountain SJ. ATP evokes Ca
837 (2+) responses and CXCL5 secretion via P2X4 receptor activa-
838 tion in human monocyte-derived macrophages. *J Immunol.*
839 2018;200:1159–68.
59. Tsien JZ, Chen DF, Gerber D, Tom C, Mercer EH, Anderson DJ,
840 et al. Subregion- and cell type-restricted gene knockout in mouse
841 brain. *Cell.* 1996;87:1317–26.
60. Stokes L, Layhadi JA, Bibic L, Dhuna K, Fountain SJ. P2X4
842 receptor function in the nervous system and current breakthroughs
843 in pharmacology. *Front Pharm.* 2017;8:291.
61. Franklin KM, Asatryan L, Jakowec MW, Trudell JR, Bell RL,
844 Davies DL. P2X4 receptors (P2X4Rs) represent a novel target for
845 the development of drugs to prevent and/or treat alcohol use
846 disorders. *Front Neurosci.* 2014;8:176.
62. Huganir RL, Nicoll RA. AMPARs and synaptic plasticity: the last
847 25 years. *Neuron.* 2013;80:704–17.
63. Baxter AW, Choi SJ, Sim JA, North RA. Role of P2X4 receptors
848 in synaptic strengthening in mouse CA1 hippocampal neurons.
849 *Eur J Neurosci.* 2011;34:213–20.
64. Pankratov YV, Lalo UV, Krishnal OA. Role for P2X receptors in
850 long-term potentiation. *J Neurosci.* 2002;22:8363–9.
65. Jo YH, Boue-Grabot E. Interplay between ionotropic receptors
851 modulates inhibitory synaptic strength. *Commun Integr Biol.*
852 2011;4:706–9.
66. Wyatt LR, Goudar SC, Khoja S, Jakowec MW, Alkana RL, Bor-
853 tolato M et al. Sociocommunicative and sensorimotor impairments
854 in male P2X4-deficient mice. *Neuropsychopharmacology.*
855 2013;38:1993–2002.

- 876 67. Mayford M, Bach ME, Huang YY, Wang L, Hawkins RD, Kandel 888
877 ER. Control of memory formation through regulated expression of 889
878 a CaMKII transgene. *Science*. 1996;274:1678–83. 890
- 879 68. Parkhurst CN, Yang G, Ninan I, Savas JN, Yates JR 3rd, Lafaille JJ, 891
880 et al. Microglia promote learning-dependent synapse formation 892
881 through brain-derived neurotrophic factor. *Cell*. 2013;155:1596–609. 893
- 882 69. Hafner S, Wagner K, Weber S, Groger M, Wepler M, McCook O, 894
883 et al. Role of the purinergic receptor P2XR4 after blunt chest 895
884 trauma in cigarette smoke-exposed mice. *Shock*. 2017;47:193–9. 896
- 885 70. Chen H, Xia Q, Feng X, Cao F, Yu H, Song Y, et al. Effect of 897
886 P2X4R on airway inflammation and airway remodeling in allergic
887 airway challenge in mice. *Mol Med Rep*. 2016;13:697–704.
- 888 71. Yang T, Shen JB, Yang R, Redden J, Dodge-Kafka K, Grady J, 889
890 et al. Novel protective role of endogenous cardiac myocyte P2X4
891 receptors in heart failure. *Circ Heart Fail*. 2014;7:510–8. 892
- 893 72. Pettengill MA, Marques-da-Silva C, Avila ML, d'Arc dos Santos
894 Oliveira S, Lam VW, Ollawa I, et al. Reversible inhibition of
895 Chlamydia trachomatis infection in epithelial cells due to stimu-
896 lation of P2X(4) receptors. *Infect Immun*. 2012;80:4232–8. 897
- 897 73. Gonzales E, Julien B, Serriere-Lanneau V, Nicou A, Doignon I,
898 Lagoudakis L, et al. ATP release after partial hepatectomy regu-
899 lates liver regeneration in the rat. *J Hepatol*. 2010;52:54–62. 900

UNCORRECTED PROOF

Journal : 41380

Article : 641

SPRINGER NATURE

Author Query Form

Please ensure you fill out your response to the queries raised below and return this form along with your corrections

Dear Author

During the process of typesetting your article, the following queries have arisen. Please check your typeset proof carefully against the queries listed below and mark the necessary changes either directly on the proof/online grid or in the 'Author's response' area provided below

Queries	Details Required	Author's Response
AQ1	Please check your article carefully, coordinate with any co-authors and enter all final edits clearly in the eproof, remembering to save frequently. Once corrections are submitted, we cannot routinely make further changes to the article.	
AQ2	Note that the eproof should be amended in only one browser window at any one time; otherwise changes will be overwritten.	
AQ3	Author surnames have been highlighted. Please check these carefully and adjust if the first name or surname is marked up incorrectly. Note that changes here will affect indexing of your article in public repositories such as PubMed. Also, carefully check the spelling and numbering of all author names and affiliations, and the corresponding email address(es).	
AQ4	You cannot alter accepted Supplementary Information files except for critical changes to scientific content. If you do resupply any files, please also provide a brief (but complete) list of changes. If these are not considered scientific changes, any altered Supplementary files will not be used, only the originally accepted version will be published.	
AQ5	Please provide the page range and volume number for references 18 and 45.	
AQ6	Please complete and update reference 52.	